Zhang, C., Laughlin, L., Beach, M., Morris, K., & Haine, J. (2016). Micro-Electromechanical impedance control for Electrical Balance Duplexing. In M. Katz (Ed.), European Wireless 2016: 22th European Wireless Conference: 18-20 May 2016, University of Oulu, Finland. [74] VDE Verlag.

Micro-Electromechanical Impedance Control for Electrical Balance Duplexing

Chunqing Zhang, Leo Laughlin, Mark A. Beach, Kevin A. Morris, and John L. Haine.
Communication Systems & Networks Laboratory, University of Bristol, UK, BS8 1UB.
Email: jack.zhang@bristol.ac.uk

***Abstract*—The Electrical Balance Duplexer (EBD) implements a form of self-interference cancellation, and can provide high Tx-Rx isolation whilst allowing simultaneous transmit (Tx) and receive (Rx) trough a single antenna in In-Band Full-Duplex (IBFD) radio transceivers. This paper presents a novel Micro-ElectroMechanical Systems (MEMS) based implementation of the tunable balancing impedance component of the EBD. A prototype MEMS tunable impedance demonstrates excellent tuning range and accuracy, and can operate over wide frequency ranges, balancing the EBD at 800 MHz and 1900 MHz to provide >40 dB isolation over a 20 MHz bandwidth. However, the MEMS tunable impedance is observed to introduce non-linear distortion into the system. This non-linearity does not significantly degrade the Tx error vector magnitude, however it has a substantial detrimental impact on the performance of a second stage of linear active cancellation, which achieved just 16 dB of additional cancellation at a Tx power of 23 dBm.**

I. Introduction

Over the coming decade, the fifth generation of mobile communication technology, 5G, is expected to deliver substantial increases in network capacity in order to meet unprecedented increases in demand. Due to the limited electromagnetic spectrum available for mobile communication, novel technologies and techniques which increase spectral efficiency will be key to meeting this demand. In-band Full-Duplex (IBFD) communication, in which devices transmit and receive on the same frequency at the same time, has been the subject of significant recent attention [1]. IBFD can provide up to double the spectral efficiency, however this is contingent on effective cancellation of the Self-Interference (SI) which results from the co-located co-channel transmitter and receiver. To mitigate the SI, many IBFD transceiver architectures and prototypes, e.g. [2], [3], have been proposed, combining various techniques which avoid or cancel SI in order to provide high transmit-to-receive (Tx-Rx) isolation.

Electrical Balance (EB) duplexing implements a form of SI cancellation. The EB Duplexer (EBD) connects the transmitter, receiver, and antenna through a hybrid junction, along with a *balancing impedance*, as depicted in Fig. 1. The ideal EBD provides high (theoretically infinite) Tx-Rx isolation when the balancing impedance is equal to the antenna impedance. However, in practice the antenna impedance is frequency variant, limiting the isolation bandwidth that can be achieved and requiring the balancing impedance to be tunable for the purposes of band selection. Furthermore, due to environmental effects, the antenna impedance may also be time variant, requiring the balancing impedance to adaptively track the antenna impedance in order to maintain isolation. A drawback of EB duplexing is high Tx and Rx insertion loss, which for a symmetrical hybrid junction, is 3 dB in both the Tx and Rx path, reducing the Tx efficiency and Rx sensitivity respectively. However, this can be mitigated by using an asymmetric hybrid junction and a noise matched receiver, with the EBD in [4] achieving a 2.2 dB Tx insertion loss and 5 dB Rx noise figure. The EBD can potentially be implemented using a Complementary Metal Oxide Semi-conductor (CMOS) process [4]–[6], and may therefore be a suitable choice for a low cost small-form-factor implementation of SI cancellation. Previously reported EBDs have implemented the tunable balancing impedance using switched resistor and capacitor arrays in CMOS [4]–[6], electromechanical impedance tuners [7], and using active methods to control the effective reflection coefficient [8].

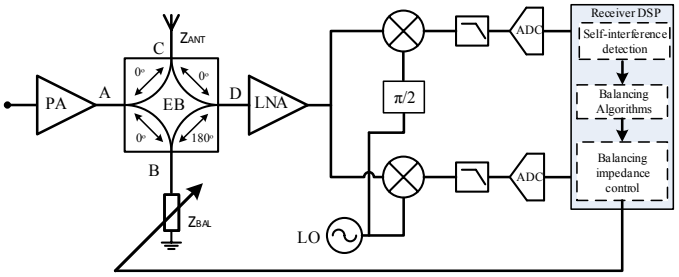

Fig. 1. Electrical Balance Duplexer (EBD) with adaptive balancing.

In recent years, Micro-ElectroMechanical Systems (MEMS) technology has an increasingly popular implementation for tunable RF components. Compared to CMOS switch capacitor arrays, MEMS tunable capacitors have the advantage of substantially higher Q factors (which reduces insertion loss) and higher voltage handling capability. MEMS components can also be fabricated on a silicon, quartz, glass, or CMOS substrate, making it suited to small factor applications.

In this paper, a novel application of MEMS technology is presented, using MEMS digitally controlled tunable capacitors to implement the tunable balancing impedance subsystem of an EBD. The balancing impedance must be capable of tolerating the high voltage swing at the PA output, and dissipating a substantial portion of the Tx power (as much as 50%), and therefore the high voltage handling capability of MEMS is a significant advantage over a CMOS implementation. Section II describes the MEMS tunable impedance implementation and section III presents the measured Tx-Rx isolation performance. Section IV analyzes the degradation in SI channel linearity and Tx path linearity due to the MEMS balancing network. Section V demonstrates the performance of a further stage of active self-interference cancellation, when combined with the MEMS balanced EBD and section VI concludes this paper.

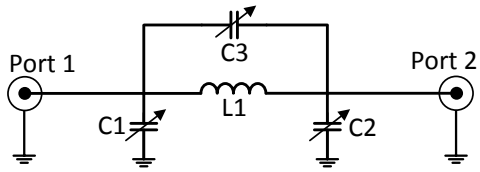

Fig. 2. π-topology impedance matching network.

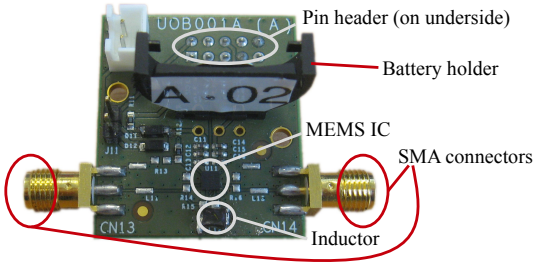

Fig. 3. Hardware implementation of the MEMS tunable balancing impedance.

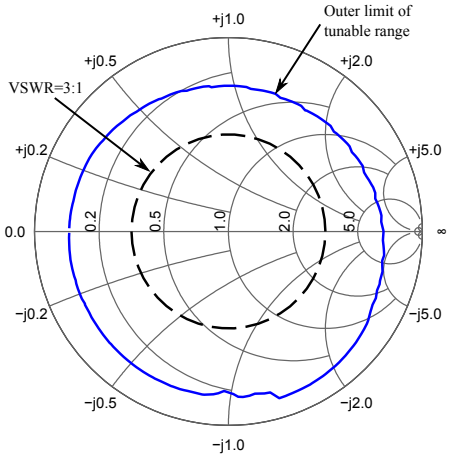

Fig. 4. Measured tunable range of the balancing impedance, showing the S_{11} values at 1.9 GHz with 216,000 states inside of the outer limit curve.

II. MEMS Balancing Network

A. Balancing Network Requirements

To balance the EBD at a particular frequency, the tunable balancing impedance must tune to the value of the antenna impedance at that frequency. The requirements for the tunable balancing impedance are therefore threefold:

1) High impedance tuning accuracy: The isolation provided by the EBD is limited by the error between the balancing and antenna impedance. Therefore *achieving high isolation requires correspondingly high balancing impedance tuning accuracy*.

2) High impedance tuning speed: Due to environmental interaction, the antenna impedance is time variant, thereby requiring the balancing impedance to adaptively adjusted to track antenna impedance variation (see Fig. 1). This is especially true in mobile devices, where interaction with the user can result in substantial antenna impedance variation, significantly reducing the Tx-Rx isolation. Previous results [9] have shown that correcting the balancing impedance at intervals of 10 ms is sufficient to maintain isolation in user interaction scenarios. When using a balancing algorithm of the type proposed in [8], the tuning time of the balancing imepdance subsystem represents a system overhead, which must therefore be minimised.

3) Wide impedance tuning range: Practical antennas exhibit significant impedance variation with frequency. Furthermore, multiband antennas may not be well matched at all operating frequencies, and in mobile handset applications a Voltage Standing Wave Ratio (VSWR) of 3:1 or lower (i.e., >6 dB return loss) is considered an acceptable match. The phase of the reflection coefficient could also take any value, depending on the design of the antenna and antenna feed, and therefore to balance the EBD, *the balancing reflection coefficient must be capable of tuning to any value within the VSWR=3:1 region of the smithchart*. Co-design of the antenna and balancing impedance could reduce the tuning range requirement, however the effect of the environment, and in particular the user's hand and head in a mobile application, can cause large fluctuations in the antenna impedance value, and therefore a significant tuning range would still be required to compensate for this effect. Antenna Tuning Units (ATUs) are now commonly deployed in mobile handset applications, and may improve the antenna match at the instantaneous operating frequency, typically reducing the VSWR to less than 2:1, which would be beneficial in terms of reducing the required tuning range of the balancing impedance, such that *the balancing impedance must be capable of tuning to any value within the VSWR=2:1 region of the smithchart if an ATU is used* [10].

B. MEMS Implementation

A MEMS tunable capacitor π-network topology for antenna impedance tuning was proposed in [11] and depicted in Fig. 2. This matching network topology is also applicable to a tunable impedance implementation: whereas the antenna tuning application transforms the antenna impedance towards 50 Ω, the topology can equally be used to transform a 50 Ω termination toward a desired impedance value.

The π-network topology of Fig. 2 was implemented using WiSpry WS1050 digitally tunable capacitors. The WS1050 Integrated Circuit (IC) contains 3 capacitors, each of which can be tuned from 0.46pF to 5.69pF in 0.1pF steps with 20μs of settling time. Circuit modelling was used to simulate the circuit in order to determine the inductor value which maximizes the tuning range (also referred to as "smithchart coverage") for this capacitor tuning range and a given operating frequency. For an operating frequency of 1.9 GHz, a 5nH off-chip air-core inductor was selected for L_1. The WiSpry WS1050 based tunable π-network PCB implementation is depicted in Fig. 3, fabricated using FR-4, and including a CR2032 battery as the DC power supply. The IC is programmed using a serial interface connected through a pin header.

A Keysight N5242A PNA-X Vector Network Analyzer (VNA) was used to measure the S_{11} of this device (reflection coefficient at Port1 when Port2 is terminated with 50 Ω). Fig. 4 plots the measured S_{11} at 1.9 GHz across all capacitor value permutations. Each tunable capacitor C_1, C_2 and C_3, has 60 tuning states, and therefore the tunable balancing impedance has a total of $60^3 = 216,000$ tuning states; Fig. 4 plots all

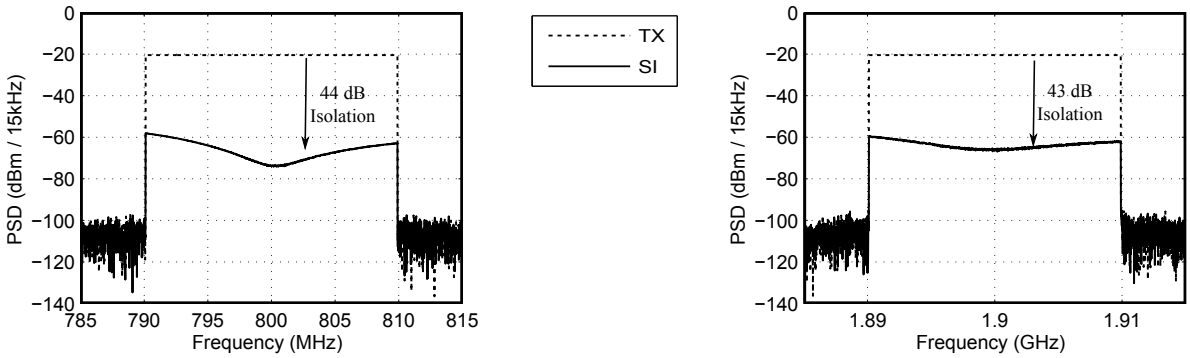

(a) 800 MHz Band (b) 1.9 GHz Band

Fig. 5. Measured EBD isolation of 20 MHz bandwidth at (a) 800 MHz Band and (b) 1.9 GHz Band.

of these states in order that the smithchart coverage can be observed. Clearly this tunable impedance circuit has excellent smithchart coverage, covering significantly more than the required VSWR 3:1 area. At 800 MHz the smithchart coverage was reduced but still covered the whole of the VSWR=2:1 region.

III. EBD Isolation Measurement

A. Experimental Setup

An EBD prototype including the MEMS based tunable balancing impedance was constructed and the performance measured. The hybrid junction used is a discrete Krytar model 1831 hybrid coupler, and a Taoglas PAD710 multiband cellular antenna was used to allow for performance comparison against previous results reported in [7]. For the Tx and Rx subsystems, a National Instruments PXIe system was used, comprising 2 PXIe-5646R Vector Signal Transceivers (VSTs) and a PXIe-8135 embedded controller, mounted in a PXIe-1085 chassis. The system was configured such that the Tx and Rx share a common LO.

An OFDM physical layer was used, thereby allowing the Tx-Rx transfer function (i.e. the self-interference channel) to be measured on a per-subcarrier basis to determine the Tx-Rx isolation frequency response. All baseband digital signal processing, including the Fast Fourier Transform (FFT) and Inverse Fast Fourier Transform (IFFT), and cyclic prefix signal processing was implemented in LabView and runs on the embedded controller. The physical layer is similar to 3GPP LTE standard using a 15 kHz sub-carrier spacing, and a sampling rate of 30.72 MHz. The operational system bandwidth (i.e. occupied sub-carriers) was 19.8 MHz, and the Tx power was 10 dBm. The system implements the balancing algorithm previously presented in [8], determining the balancing impedance settings required to balancing the EBD in order to maximise the isolation at the centre of the band.

B. Isolation Results

The Tx-Rx isolation was measured at two carrier frequencies: 800 MHz and 1900 MHz. Results are plotted in Fig. 5, which shows the Power Spectral Density (PSD) of Tx signal and residual SI at the receiver input, demonstrating substantial isolation across the band. Table I reports the mean isolation across the 20 MHz bandwidth, and compares this against results previously reported in [7] and [12]. The system in [7] is identical to the system discussed here, but uses a laboratory instrumentation type electromechanical impedance tuner instead of the MEMS device, and thus these results allow for direct comparison of the two balancing impedance implementation methods. The two systems achieve very similar isolation performance of 43 - 45 dB for all combinations of frequency and tunable impedance implementation. The EBD subsystem in [12] is implemented by CMOS process with switch controlled balancing impedance. Comparing with [12], this paper's implementation achieves more bandwidth (BW) at the similar isolation figures.

TABLE I. Comparison of measured TX-RX isolation against mechanical tuner and CMOS circuits

Reference	Freq.	Balancing Network	Mean Isolation
This work, 20MHz BW	800 MHz	MEMS Circuit	EBD = 44 dB
This work, 20MHz BW	1900 MHz	MEMS Circuit	EBD = 43 dB
[7], 20MHz BW	890 MHz	Mechanical Tuner	EBD = 44 dB
[7], 20MHz BW	1890 MHz	Mechanical Tuner	EBD = 45 dB
[12], 6MHz BW	2450 MHz	CMOS	EBD = 50 dB
[12], 10MHz BW	2450 MHz	CMOS	EBD = 44 dB

Result 1: MEMS tunable capacitors can be used to implement the tunable balancing impedance of an EBD without a significant impact on the linear self-interference transfer function at a 10 dBm input power.

Result 2: The MEMS tunable impedance can operate over wide frequency ranges, maintaining the tuning range and tuning accuracy required for the EBD balancing application.

IV. Non-linearity Measurement

Although the linear Tx-Rx isolation was substantially unaffected by the MEMS implementation as compared to the mechanical tuner, any non-linear characteristics in the MEMS components may affect the Tx path linearity, potentially degrading the Tx Error Vector Magnitude (EVM), and the self-interference channel linearity, which may increase the requirement for non-linear cancellation in further stages of SI cancellation. The SI cancellation in an EBD is contingent on equal reflection coefficients at the antenna port (the antenna reflection coefficient) and the balance port (i.e. the balancing reflection coefficeint). Any non-linear characteristics in the balancing reflection will produce non-linear components which will not be cancelled (cancelling this would require an identical

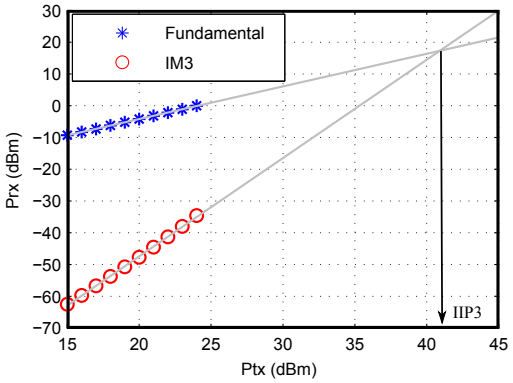

Fig. 6. Measured IIP3 of EBD with MEMS balancing network at 1.9 GHz

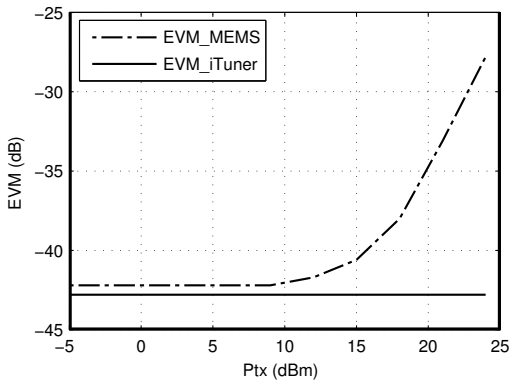

Fig. 7. The estimated relative magnitude of the non-linear distortion introduced into the self-interference at the EBD Rx port.

non-linearity at the antenna port), resulting in a non-linear self-interference channel through the EBD. To quantify this, the third order input intercept point (IIP3) of the S_{11} of the MEMS tunable balancing impedance was measured, and the in-band distortion introduced in the Tx path and the EBD self-interference channel was also measured, comparing the linearity and resulting distortion observed in the MEMS EBD against the linear electromechanical tuner implementation.

A. Balancing Circuit IIP3 Measurement

The IIP3 of the balancing port reflection coefficient was measured using a two tone test. The two Carrier Wave (CW) sources were used to generate two CW tones centred at 1.9 GHz and with a 5 MHz spacing. The output of each CW source was isolated using a circulator, and the two signals were then combined using a directional coupler to generate the two tone signal. A second directional coupler was then used to separate the incident and reflected signals at port 1 of the MEMS tunable impedance, with the two tone signal being fed into the tunable impedance network, and the reflected signal being fed to a spectrum analyser, such that the power of the fundamental and third order intermodulation (IM3) components could be measured. As is the case in the EBD balancing application, port 2 of the tunable impedance was terminated with 50 Ω. Fig. 6 plots the power of the fundamental and IM3 components as the input power was swept from 15 dBm to 24 dBm, and as shown from this the IIP3 can be estimated as 41 dBm. Similar measurement was done at 800 MHz in which a much higher IIP3 of 51 dBm was achieved. As would be expected considering result 1, this meets the balancing reflection coefficient linearity requirement as derived in [10], where it is shown that the balancing reflection coefficient requires an IIP3 of 44.5 dBm in order to prevent un-cancelled non-linear residual self-interference from reducing EBD isolation below 50 dB, up to a maximum Tx power of 27 dBm.

B. Distortion measurement

To quantify the non-linear distortion introduced into the self-interference channel by the balancing impedance, an EVM estimation technique was applied to the residual self-interference at the EBD output. The EVM was estimated by measuring the linear Tx-Rx channel. The linear channel estimation was performed at low power such that non-linear distortion was negligible, and the channel estimate was averaged across many measurement to provide a high signal-to-noise ratio estimate of the linear component of the self-interference channel. Using the linear channel estimate, the linear residual self-interference could then be calculated from the Tx signal, and by comparing this to the measured SI, the distortion could be estimated. For example, the SI at the EBD output, $S_I(\omega)$, can be expressed as the sum of a linear self-interference component, $S_{I_{lin}}(\omega)$, and a distortion component, $D(\omega)$, such that

$$S_I(\omega) = S_{I_{lin}}(\omega) + D(\omega). \tag{1}$$

The linear self-interference component is the product of the Tx signal, $S_T(\omega)$, and the linear EBD Tx-Rx transfer function, $C_{EBD}(\omega)$, such that

$$S_{I_{lin}}(\omega) = S_T(\omega) C_{EBD}(\omega). \tag{2}$$

$C_{EBD}(\omega)$ is measured at low power to yield an estimate, $\hat{C}_{EBD}(\omega)$. Using this, the distortion can be estimated as

$$\begin{aligned} \hat{D}(\omega) &= S_I(\omega) - \hat{S}_{I_{lin}}(\omega) \\ &= S_I(\omega) - S_T(\omega)\hat{C}_{EBD}(\omega). \end{aligned} \tag{3}$$

The EVM is then calculated as

$$\text{EVM} = \frac{\overline{|D(\omega)|^2}}{\overline{|S_I(\omega)|^2}}. \tag{4}$$

The accuracy of this EVM estimate is affected by the EVM of the Tx chain, and noise in the measurements. However, as will be clear from the results, the distortion introduced by the MEMS tunable impedance system becomes the dominant distortion component, and thus the distortion from noise and the Tx chain becomes negligible at higher Tx powers. The measurements and signal processing required to implement this estimation technique were implemented on the NI VST platform as described in section III.A, at a carrier frequency of 1.9 GHz as the Tx power was swept from -5 dBm to 24 dBm. To increase the Tx power, the VST Tx output was connected to the EBD Tx port through a MILMEGA linear power amplifier. In order to remove and dependence of the linearity of the the signal source (the VST Tx and amplifier), the output power of the VST, was fixed and the input power to the EBD was controlled using variable attenuators, such that any non-linear

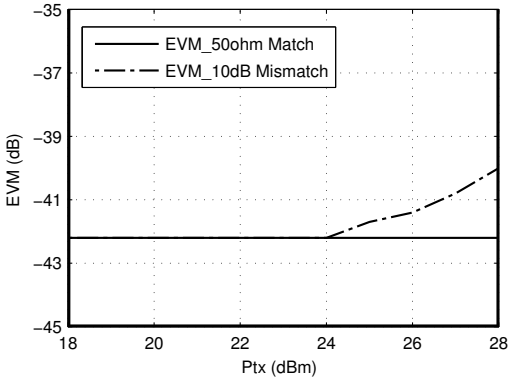

Fig. 8. Transmit signal error vector magnitude at the EBD antenna port for matched and mismatched Rx port impedances.

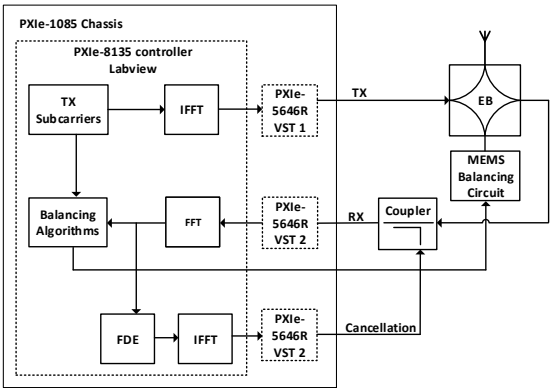

Fig. 9. Two stages IBFD architecture. The first stage is passive EB and the second stage is active cancellation in which cancellation signal is generaged by another predistorted auxiliary PA.

distortion power present in the input signal remains at a fixed ratio with the total input signal power. This Tx chain was observed to be highly linear, achieving an EVM of less than (<-40 dB).

Results are plotted in Fig. 7, showing the estimated EVM for the self-interference in the MEMS implementation and the mechanical tuner ("iTuner") implementation. Below 10 dBm, the distortion caused by the MEMS tunable impedance circuit is below that of the Tx chain, and therefore there is no change in EVM as the input power is swept. However, for input powers above 10 dBm, the non-linear distortion from the MEMS balancing circuit becomes the dominant distortion component in the residual SI signal, and increases the EVM estimate. The implementation using the linear mechanical tuner shows no increase in distortion. Since the only difference between the two systems is the tunable balancing impedance implementation, the additional distortion observed in the MEMS based implementation must be from the MEMS tunable balancing impedance circuit.

Result 3: The MEMS tunable balancing impedance network can introduce significant non-linear distortion into the residual self-interference.

Non-linear distortion introduced into the Tx signal was also measured using the same method. Tx path distortion occurs when signals reflected at the balance port couple to the antenna port. In the ideal EBD, the antenna and balance ports are isolated, however coupling between these ports is increased when the impedances at the Tx and Rx port are not identical (as would be the case, for example, if a noise matched receiver design is employed [4]), thereby coupling distortion to the antenna port.

Fig. 8 plots the Tx EVM measured at the antenna port when the Tx and Rx ports are perfectly matched, and when the Rx port is mismatched with a reflection coefficient magnitude of -10 dB. Where the ports are matched, no distortion is coupled to the antenna port and the Tx EVM is not degraded by the balancing impedance non-linearity. However, when the receiver is mismatched, additional Tx distortion was observed at power levels above 24 dBm. However, up to power levels of 28 dBm, the total EVM of the Tx signal was <-40 dBm, exceeding the performance of typical power amplifiers in mobile devices. Therefore, although this distortion is detectable in this laboratory setup, in a practical low cost radio system, this additional distortion will not be significant in comparison to other sources of Tx distortion (i.e. the rest of the Tx chain).

Result 4: Mismatch at the Tx and/or Rx port can result in non-linear distortion being coupled to the antenna port.

Result 5: The degradation in Tx EVM in a MEMS balanced EBD is not significant compared other sources of Tx distortion in mobile device applications.

V. Active Self-Interference Cancellation

The results and analysis presented hitherto have demonstrated that the MEMS tunable balancing impedance can introduce significant non-linearity into the EBD self-interference channel. Although this distortion is not powerful enough to compromise the EBD Tx-Rx isolation at Tx powers common in mobile devices (i.e. <30 dBm), the in-band non-linear distortion present in the residual self-interference is highly relevant to the design and performance of further stages of self-interference cancellation. The non-linear distortion in the SI at the EBD output cannot be cancelled using further stages of linear SI cancellation, and can only be suppressed using non-linear signal processing, which can be significantly more complex and computationally expensive.

To quantify the impact on the performance of further stages of linear cancellation, the EBD with MEMS tunable balancing impedance was combined with a further stage of linear active cancellation. The NI VST based hardware implementation described in section III.A was augmented to include a second auxiliary transmitter for the purposes of active cancellation signal generation. This is essentially the same Electrical Balance and Active Cancellation (EBAC) prototype as previously presented in [7]. The baseband signal processing for cancellation signal generation is performed in the embedded controlled, generating a digital baseband cancellation signal which is then up-converted and injected at the EBD output using a directional coupler, as shown in Fig. 9. Full details of the experimental setup can be found in [7].

Fig. 10 plots the residual SI at the EBD output ("SI-EB only"), and after the second stage of active cancellation ("SI-EBAC"), for three different input power levels, and the mean isolation values for these measurements are given in Table II. The results clearly demonstrate that the active cancellation stage provides less cancellation at higher power levels, this

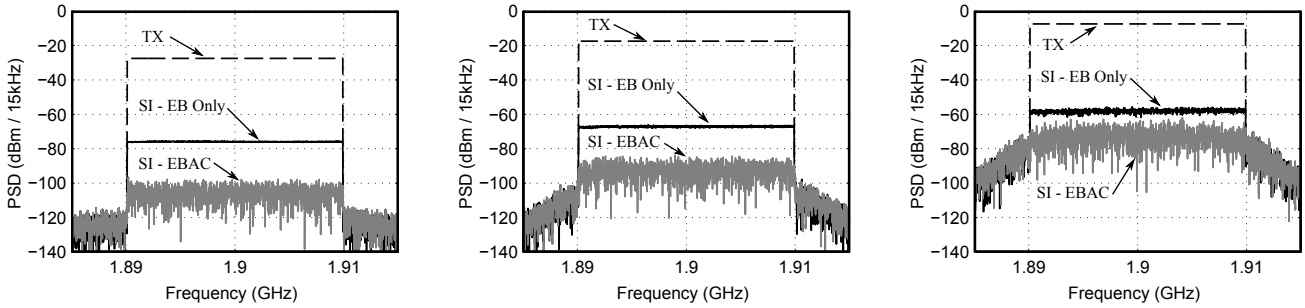

(a) TX power at 3 dBm (b) TX power at 13 dBm (c) TX power at 23 dBm

Fig. 10. Self-interference power spectra density when using passive SI cancellation (the EBD), Active RF cancellation, and when combining passive and active cancellation for three Tx power levels: (a) 3 dBm Tx power. (b) 13 dBm Tx power. (c) 23 dBm Tx power.

TABLE II. MEASURED SI CANCELLATION PERFORMANCE FOR THREE TX POWER LEVELS (MEAN OVER 20 MHZ BANDWIDTH).

TX Power	Isolation, EB only	Active cancellation	Total isolation (EBAC)
3 dBm	48 dB	30 dB	78 dB
13 dBm	49 dB	26 dB	75 dB
23 dBm	49 dB	16 dB	65 dB

being due to increase in un-cancellated non-linear distortion at higher power levels.

Result 6: Non-linear distortion introduced by the MEMS balanced EBD at high power level can substantially reduce the effectiveness of further stages of linear SI cancellation.

Therefore, for low power applications, e.g. some near field sensor networks, compound EBD subsystem and baseband digital cancellation may provide enough SI isolation. On the contrary, for high power applications, e.g. mobile handsets, AC is essential to prevent the receiver from saturating. At the same time, much more complicated non-linear digital cancellation will be necessary to model the channel and compensate the extra non-linear distortion introduced by EBD subsystem.

VI. CONCLUSION

This paper has presented a novel MEMS tunable capacitor based implementation of the tunable balancing impedance component of an Electrical Balance Duplexer. A prototype has demonstrated excellent smithchart coverage, tuning speed, tuning accuracy, and is capable of balancing the EBD at 800 MHz and 1.9 GHz.

The linearity of the MEMS implementation has been measured. The MEMS tunable impedance has a reflection coefficient IIP3 of 41 to 51 dBm. Even when the receiver port is mismatched, this non-linearity does not significantly impact on the Tx EVM. However, the distortion introduced by the MEMS tunable impedance does have a substantial impact on the self-interference channel, introducing non-linear distortion into the residual self-interference at the EBD output, thereby reducing the performance of a second stage of active linear SI cancellation, improving the complexity of digital cancellation.

ACKNOWLEDGMENT

This project is supported by the UK EPSRC through the University of Bristol Impact Acceleration Account (EP/K503824/1), CDT Equipment Award (EP/K035746/1) and u-blox AG. The authors would like to thank Balakumar Swaminathan of u-blox for helping set up the test bed.

REFERENCES

[1] A. Sabharwal, P. Schniter, D. Guo, D. W. Bliss, S. Rangarajan, and R. Wichman, "In-band full-duplex wireless: Challenges and opportunities," *Selected Areas in Communications, IEEE Journal on*, vol. 32, no. 9, pp. 1637–1652, 2014.

[2] M. Duarte and A. Sabharwal, "Full-duplex wireless communications using off-the-shelf radios: Feasibility and first results," in *Signals, Systems and Computers (ASILOMAR), 2010 Conference Record of the Forty Fourth Asilomar Conference on*. IEEE, 2010, pp. 1558–1562.

[3] D. Bharadia, E. McMilin, and S. Katti, "Full duplex radios," in *ACM SIGCOMM Computer Communication Review*, vol. 43, no. 4. ACM, 2013, pp. 375–386.

[4] M. Mikhemar, H. Darabi, and A. A. Abidi, "A multiband rf antenna duplexer on cmos: Design and performance," *Solid-State Circuits, IEEE Journal of*, vol. 48, no. 9, pp. 2067–2077, 2013.

[5] S. H. Abdelhalem, P. S. Gudem, and L. E. Larson, "Hybrid transformer-based tunable differential duplexer in a 90-nm cmos process," *Microwave Theory and Techniques, IEEE Transactions on*, vol. 61, no. 3, pp. 1316–1326, 2013.

[6] B. van Liempd, B. Hershberg, K. Raczkowski, S. Ariumi, U. Karthaus, K.-F. Bink, and J. Craninckx, "A+ 70dbm iip3 single-ended electrical balance duplexer in 0.18 μm soi cmos," in *IEEE International Solid-State Circuits Conference-ISSCC*, 2015, pp. 32–33.

[7] L. Laughlin, C. Zhang, M. A. Beach, K. A. Morris, and J. Haine, "A widely tunable full duplex transceiver combining electrical balance isolation and active analog cancellation," in *Vehicular Technology Conference (VTC Spring), 2015 IEEE 81st*. IEEE, 2015, pp. 1–5.

[8] L. Laughlin, C. Zhang, M. A. Beach, K. A. Morris, and J. L. Haine, "Passive and active electrical balance duplexers," *Circuits and Systems II: Express Briefs, IEEE Transactions on*, vol. 63, no. 1, pp. 94–98, 2016.

[9] L. Laughlin, M. A. Beach, K. A. Morris, and J. L. Haine, "Electrical balance duplexing for small form factor realization of in-band full duplex," *IEEE Communications Magazine*, vol. 53, no. 5, pp. 102–110, May 2015.

[10] S. H. Abdelhalem, P. S. Gudem, and L. E. Larson, "Tunable cmos integrated duplexer with antenna impedance tracking and high isolation in the transmit and receive bands," *Microwave Theory and Techniques, IEEE Transactions on*, vol. 62, no. 9, pp. 2092–2104, 2014.

[11] Q. Gu, J. R. De Luis, A. S. Morris III, and J. Hilbert, "An analytical algorithm for pi-network impedance tuners," *Circuits and Systems I: Regular Papers, IEEE Transactions on*, vol. 58, no. 12, pp. 2894–2905, 2011.

[12] B. Debaillie, D.-J. van den Broek, C. Lavin, B. van Liempd, E. A. Klumperink, C. Palacios, J. Craninckx, B. Nauta, and A. Parssinen, "Analog/rf solutions enabling compact full-duplex radios," *Selected Areas in Communications, IEEE Journal on*, vol. 32, no. 9, pp. 1662–1673, 2014.